Lighting up multipolar surface plasmon polaritons by collective resonances in arrays of nanoantennas

V. Giannini,* G. Vecchi, and J. Gómez Rivas
Center for Nanophotonics, FOM Institute AMOLF, c/o Philips Research Laboratories, High Tech Campus 4, 5656 AE Eindhoven, The Netherlands.

We demonstrate the coupling of multipolar surface plasmons with photonic modes in periodic arrays of metallic nanoantennas. This coupling leads to sharp resonances known as lattice surface modes. In spite of the weak interaction of multipolar surface plasmons with light, lattice surface modes provide an efficient radiative decay channel for emitters in the proximity of the array. We observe a 10-fold emission enhancement of dyes coupled to lattice resonances. Lattice surface modes light up multipolar plasmonic resonances, opening new possibilities for fluorescence spectroscopies.

As highlighted by E. M. Purcell, the spontaneous decay rate of an optical emitter depends on the photonic density of states [1], which can be modified by its environment. Optical nanoantennas are excellent examples of structures enabling control of the light emission at the nanoscale [2, 3]. Through the excitation of localized surface plasmon resonances (LSPRs) nanoparticles can act as antennas at optical and near-infrared frequencies [4]. LSPRs lead to large local field enhancements and to a modification of the photonic density of states, i.e., a modification of the decay rate, as well as the directionality of the emission from emitters positioned close to nanoantennas [5–9].

The efficient optical excitation of LSPRs in small nanoparticles is possible because of their dipolar character [10, 11]. These resonances are known as bright LSPRs in contrast to multipolar LSPRs, which couple marginally to light for beyond the quasi-static limit due to retardation effects [10]. Calculations beyond the quasi-static approximation have shown that dipoles in the proximity of nanoparticles can excite multipolar LSPRs in addition to dipolar resonances, leading to a significant modification of the dipole decay rate[10–14]. The effect of multipolar resonances is a strong reduction of the emission efficiency, which can be understood as follows: light emitters can decay exciting multipolar LSPRs that do not couple efficiently to far-field radiation and are quenched due to Ohmic losses in the metal. Also, emission quenching is expected when multipolar resonances are spectrally close to dipolar resonances [14, 15].

In this Letter we demonstrate that the coupling of multipolar LSPRs of nanoantennas with diffractive orders in periodic arrays or plasmonic crystals (PCs) of these nanoantennas, makes possible the efficient excitation of lattice surface modes (LSMs). Despite the fact that these lattice resonances originate from multipolar LSPRs, they couple very efficiently to radiation due to their hybrid plasmonic-photonic character. LSMs represent an important new decay channel for emitters and open routes for the design of nanostructured surfaces to control the spontaneous emission.

LSMs were predicted by Carron and co-workers [16] and Markel [17]. PCs of nanoparticles can support collective resonances arising from the coupling of LSPRs with diffracted orders grazing to the crystal surface, i.e., with Rayleigh anomalies. A new physical insight into this phenomenon was given by Schatz and co-workers [18] by showing theoretically that coherent dipolar interactions in nanoparticle arrays can give rise to sharp resonances. These resonances result from the partial cancelation of the damping associated with the single particle resonance. LSMs on PCs were proposed by Garcia de Abajo and co-workers [19] as an explanation for the enhanced optical transmission through arrays of subwavelength holes on metallic films [20]. Despite the long time since the first theoretical work on these collective excitations, they were only very recently demonstrated experimentally [21–25]. All theoretical and experimental work so far has focused on the coherent dipolar coupling as mechanism for the excitation of these collective resonances. This is in contrast to the results presented here, where we demonstrate their excitation through the coupling of multipolar resonances.

A PC with dimensions 3×3 mm^2 of gold nanoantennas was fabricated on a glass (AF45) substrate using substrate conformal imprint lithography [26]. The nanoantennas have a rectangular shape with a height of 38 ± 2 nm, a long axis of 450 ± 15 nm along the x direction and a short axis of 130 ± 15 nm along the y direction (see Fig. 1). The α and θ angles in Fig. 1(a) define the angles of incidence. The lattice constants of the PC are $a_x = 600 \pm 15$ nm and $a_y = 300 \pm 15$ nm. A scanning electron microscope (SEM) image of the sample is shown in Fig. 1(b). A layer of thickness 50 ± 10 nm, containing fluorescent molecules (ATTO 680) dispersed into a polyvinyl butyral (PVB) matrix with a concentration of 10^{-5} M, was spun onto the array.

In order to understand the resonances of the array, we have first calculated the extinction cross section of individual nanoantennas (see Fig. 1(c)) using the Finite Difference on Time Domain method. To simplify the calculations we approximate the nanoantennas as being in an homogeneous background with refractive index $n = 1.5$. These calculations were done for angles of inci-

dence $\alpha = \theta = 0^\circ$ (red dashed curve) and $\alpha = 0^\circ, \theta = 20^\circ$ (blue solid curve). The incident electric field is polarized along the long nanoantenna axis. The plasmonic resonances are identified by the maxima in the extinction cross section, and approximated by the relation: $L \simeq j\frac{\lambda_{eff}}{2}$, where λ_{eff} is the effective wavelength in the nanoantenna [27], j is an integer that gives the resonance order and L is the nanoantenna length along the direction of the polarization vector. The $j = 1$ resonance corresponds to the dipolar resonance and it is characterized by a low Q-factor (broad resonance) and a large extinction cross section. These two features are a consequence of the good coupling of this resonance to light. Multipolar resonances ($j > 1$) exhibit a lower extinction cross section and are narrower than the dipolar resonance due to their weaker coupling to light and reduced radiation damping.

When light impinges from the top at an angle $\alpha = 0^\circ$ only odd resonance orders, with an antisymmetric charge distribution along the long nanoantenna axis, can be excited [28]. This selection rule is only valid for $\alpha = 0^\circ$ since the electric field has even parity with respect to the center of the nanoantenna. Note that if the angle θ is different than zero but $\alpha = 0^\circ$ still only odd resonances can be excited because the electric field is symmetric with respect to the center of the nanoantenna along the x direction. The odd resonances for $\alpha = \theta = 0^\circ$ are clear in Fig. 1(c), where the dipolar or $\lambda/2$ resonance (first order) and the $3\lambda/2$ resonance (third order) are excited around $\lambda = 1750$ nm and $\lambda = 750$ nm respectively. Due to the strong reduction of radiation losses in multipolar resonances, the Q-factor of the $3\lambda/2$ resonance, $Q \simeq 11$, is seven times larger than the Q-factor of the $\lambda/2$ resonance. Therefore, the $3\lambda/2$ resonance can be considered as a quasi-dark resonance, which couples weakly to radiation [10, 11]. By varying the angle of incidence from the normal to $\alpha = 0^\circ$ and $\theta = 20^\circ$ (electric field along x, wavevector in the (y, z) plane) the odd resonances show a decrease in strength. The first even order resonance, i.e., the $j = 2$, appears when the incident electric field is not symmetric along the long nanoantenna axis, i.e., for $\alpha \neq 0^\circ$ (not shown).

Figure 1(d) shows a calculation of the extinction, which we define as one minus the transmittance, of the nanoantenna array on a glass substrate covered by a layer of PVB with a thickness of 50 nm. It has been recently shown in Ref. [24] that a thin dielectric layer on top of the nanoantenna array is sufficient for an efficient coupling of LSPRs in the nanoantennas to diffractive orders of the array. A blue-shift of the dipolar resonance of the nanoantennas is found when they are arranged in the array [29]. In contrast to the dipolar resonance, the $3\lambda/2$ resonance in the array does not present substantial shift with respect to the resonance of individual antennas. More interestingly, a sharp resonance in the extinction appears around $\lambda = 900$ nm for $\theta = 20^\circ$ (blue curve in Fig. 1(d)). This resonance is the LSM resulting from the coupling of the $3\lambda/2$ resonances of individual nanoantennas with a diffracted wave propagating grazing to the surface of the array.

A close view of the spectral region around the lattice surface resonance is displayed in Fig. 2(a) and compared with measurements in Fig. 2(b). The measurements were done by illuminating the sample with the collimated beam from a halogen lamp with a diameter of 1 mm and normalizing the transmission spectrum by the transmission through a bare substrate. Excellent agreement is obtained between simulations and measurements. The arrows in figure 2(b) indicate the minima in the extinction at the wavelengths at which diffracted orders become evanescent, i.e., the Rayleigh anomalies. At normal incidence, $\alpha = \theta = 0^\circ$, only the $3\lambda/2$ LSPR and a minimum due to the Rayleigh anomaly are visible in the extinction spectrum. For the angle of incidence $\alpha = 0^\circ$, $\theta = 20^\circ$ the sharp peak associated to the LSM appears at a wavelength red-shifted with respect to the Rayleigh anomaly.

We have also performed angular resolved extinction measurements to determine the dispersion of multipolar LSMs. We rotate the sample around the x-axis, varying the angle θ in the range $0^\circ - 50^\circ$, while keeping $\alpha = 0^\circ$. These measurements are displayed in Fig. 3(a) as a function of the normalized frequency ω/c and the wavevector parallel to the surface of the nanonantenna array, i.e., $k_{\|} = (2\pi/\lambda)\sin(\theta)$. The resonance centered around $\omega/c = 8$ mrad nm^{-1} corresponds to the $3\lambda/2$ LSPR. The localized character of this resonance to the individual nanoantennas results on its flat dispersion. The band of high extinction at frequencies between 6.8 and 8 mrad nm^{-1} corresponds to the LSM. In Fig. 3(a) are also indicated the degenerate hyperbolic $(0, \pm 1)$ Rayleigh anomaly with a black solid curve. The Rayleigh anomaly is apparent in the measurements by a relative minimum in the extinction. Note that the LSM has a lower energy than the Rayleigh anomaly. Another characteristic of the collective resonance is its broadening as it approaches in frequency the $3\lambda/2$ LSPR. This broadening arise from the stronger localization of the LSM mode to the individual nanoantennas, which leads to an increase of Ohmic losses.

As it is apparent in Figs. 2 and 3(a), the LSM vanishes when the angle of incidence θ is zero ($k_{\|} = 0$). This different behavior with respect to LSMs originating from dipolar LSPRs [24, 25] provides an important information on the symmetry of the mode. In order to couple polarized radiation along the long axis of the antennas at normal incidence to a mode in the array, it is necessary that the scattered electric field is symmetric with respect to the (x, z) plane intersecting the antennas. This symmetry is imposed by the symmetry of the incident plane wave with respect to the plane defined by its wave vector and polarization. Therefore, the vanishing extinction of the

LSM at normal incidence observed in the measurements and simulations indicates that incident light cannot couple to the mode because its antisymmetric character with respect to this plane.

We have confirmed the antisymmetric field distribution of the LSM with simulations of the near field in the horizontal plane intersecting the antennas at the height of 20 nm. These calculations have been done at $\lambda = 895$ nm for an angle of incidence of $\theta = 20°$ (red point in Fig. 3(a)). The out-of-normal incidence breaks the symmetry and allows for coupling of the incident field to the LSM. This coupling gives rise to the field distribution displayed in Fig. 3(b). As can be appreciated in this figure, the field associated to the LSM is antisymmetric with respect to the vertical plane (x, z) intersecting the antennas through their long axis (red dashed lines in Fig. 3(b)). For normal incidence we expect no coupling of the incident plane wave with the LSM due to a fully symmetric field distribution associated to the incident field. It is interesting to compare the field distribution of an isolated antenna at the frequency of the $3\lambda/2$ resonance with the LSM. As can be seen in Fig 3(c), the field of the $3\lambda/2$ resonance exhibits a four-lobed (multipolar) distribution, while the surface lattice resonance presents a two-lobed (dipolar-like) distribution. This modification in the field distribution is the result of electrodynamic retardation between the $3\lambda/2$ resonances and the field diffracted in the plane of the array. As a result of this retardation, the coupling of the multipolar resonances to radiation in certain directions becomes dominant, which, as it is shown below, leads to enhancement of the emission.

We have investigated the fluorescence enhancement of dye molecules embedded in the PVB layer that covers the nanoantennas. These measurements, normalized by the fluorescence of a similar dye and PVB layer but on the absence of nanoantennas, are displayed in Fig. 4(a). The measurements were performed by illuminating the sample at $\lambda = 690$ nm at an angle $\theta = 50°$ and with a polarization parallel to the long axis of the nanoantennas. The power density of the laser incident was low enough to avoid saturation and photo-bleaching of the dye. The measurements of Fig. 4(a) correspond to the angles of detection $\alpha = \theta = 0°$ (black squares) and $\alpha = 0°$, $\theta = 20°$ (red circles). For sake of comparison, we plot in Fig. 4(b) the extinction measurements of the same array. We observe a 10-fold enhancement of the fluorescence for $\alpha = 0°$, $\theta = 20°$ at $\lambda = 930$ nm. This pronounced enhancement can be attributed to the decay of the excited dye molecules into the LSM and the coupling of this surface mode to radiation by scattering in the periodic array of nanoantennas. It is important to stress that multipolar modes couple weakly to light [10, 11]. A different scenario result from the diffractive coupling of multipolar LSPRs, namely the enhancement of the emission of fluorophores.

The spectral sharpness of LSMs allows us to determine that the maximum of the fluorescence enhancement (Fig. 4(a)) is red-shifted with respect to the maximum of extinction (Fig. 4(b)). This shift is 15 nm for $\theta = 20°$ and increases for larger values of θ (not shown). This effect is attributed to the red-shift of resonances in the near-field, where the dyes are located, with respect to the far-field resonances [30–33]. It is interesting to note that for $\alpha = \theta = 0°$ there is a small increase of the fluorescence enhancement at 910 nm (black squares in Fig. 4(a)). We attribute this residual enhancement of the fluorescence to the decay of the dye molecules to the Rayleigh anomaly, which is apparent as the minimum in the extinction measurements of Fig. 4(b).

In conclusion, we have demonstrated that arrays of gold nanoantennas support LSMs resulting from the coupling of multipolar plasmonic resonances with Rayleigh anomalies. In spite of the weak coupling of multipolar resonances to radiation, LSMs originating from multipolar resonances can enhance significantly the emission of fluoropheres. In particular, we have measured a 10-fold enhancement of the emission of dye molecules coupled to lattice surface resonances that arise from the diffractive coupling of $3\lambda/2$ antenna resonances. This enhancement opens new possibilities for fluorescence spectroscopies, e.g., large nanoantennas, which are easy to fabricate, can be used to enhance signals at shorter wavelengths through the coupling of high-order multipolar plasmonic resonances in arrays.

We thank M. Verschuuren and Y. Zhang for the fabrication of the samples. This work was supported by the Netherlands Foundation Fundamenteel Onderzoek der Materie (FOM) and the Nederlandse Organisatie voor Wetenschappelijk Onderzoek (NWO), and is part of an industrial partnership program between Philips and FOM.

* v.giannini@imperial.ac.uk

[1] E. M. Purcell, Phys. Rev. **69**, 681 (1946).
[2] P. Mühlschlegel *et al.*, Science **308**, 1607 (2005).
[3] W. E. Moerner *et al.*, Nature Photon. **3**, 654 (2009).
[4] W. L. Barnes, A. Dereux, and T. W. Ebbesen, Nature **424**, 824 (2003).
[5] S. Kühn *et al.*, Phys. Rev. Lett. **97**, 017402 (2006).
[6] P. Anger, P. Bharadwaj, and L. Novotny, Phys. Rev. Lett. **96**, 113002 (2006).
[7] O. L. Muskens *et al.*, Nano Lett. **7**, 2871 (2007).
[8] T. H. Taminiau *et al.*, Nature Photon. **2**, 234 (2008).
[9] G. Baffou *et al.*, Phys. Rev. B **77**, 121101 (2008).
[10] P. Nordlander and C. Oubre, Nano Lett. **4**, 899 (2004).
[11] M.-W. Chu *et al.*, Nano Lett. **9**, 399 (2009).
[12] J.-Y. Yan *et al.*, Phys. Rev. B **77**, 165301 (2008).
[13] M. Liu *et al.*, Phys. Rev. Lett. **102**, 107401 (2009).
[14] H. Mertens and A. Polman, J. Appl. Phys. **105**, 044302 (2009).
[15] C. P. Burrows and W. L. Barnes, Opt. Express **18**, 3187

(2010).
[16] K. T. Carron *et al.*, J. Opt. Soc. Am. B **3**, 430 (1986).
[17] V. A. Markel, J. Mod. Opt. **40**, 2281 (1993).
[18] S. Zou, N. Janel, and G. C. Schatz, J. Chem. Phys. **120**, 10871 (2004).
[19] F. J. García de Abajo, R. Gómez-Medina, and J. J. Sáenz, Phys. Rev. B **72**, 016608 (2005).
[20] T. W. Ebbesen *et al.*, Nature **391**, 667 (1998).
[21] V. Kravets, F. Schedin, and A. Grigorenko, Phys. Rev. Lett. **101**, 087403 (2008).
[22] B. Auguié and W. L. Barnes, Phys. Rev. Lett. **101**, 143902 (2008).
[23] Y. Chu *et al.*, Appl. Phys. Lett. **93**, 181108 (2008).
[24] G. Vecchi, V. Giannini, and J. G. Rivas, Phys. Rev. Lett. **102**, 146807 (2009).
[25] G. Vecchi, V. Giannini, and J. G. Rivas, Phys. Rev. B **80**, 201401 (2009).
[26] M. Verschuuren and H. van Sprang, Mater. Res. Soc. Symp. Proc. **1002-N03–05** (2007).
[27] L. Novotny, Phys. Rev. Lett. **98**, 266802 (2007).
[28] V. Giannini and J. A. Sánchez-Gil, J. Opt. Soc. Am. A **24**, 2822 (2007).
[29] L. Zhao, K. L. Kelly, and G. C. Schatz, J. Phys. Chem. B **107**, 7343 (2003).
[30] B. J. Messinger *et al.*, Phys. Rev. B **24**, 649 (1981).
[31] M. Thomas, J.-J. Greffet, and R. Carminati, Appl. Phys. Lett. **85**, 3863 (2004).
[32] P. Bharadwaj and L. Novotny, Opt. Express **15**, 14266 (2007).
[33] G. W. Bryant, F. J. G. de Abajo, and J. Aizpurua, Nano Lett. **8**, 631 (2008).

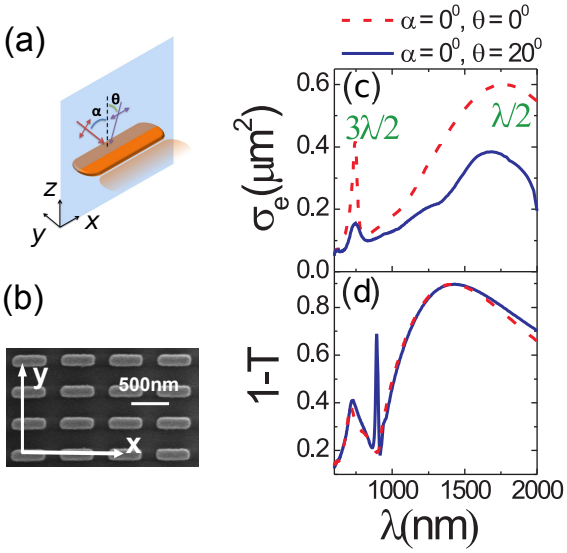

FIG. 1. (a) Schematic representation of a single nanoantenna. (b) SEM image of an array of nanoantennas. (c) Extinction cross section of a single gold nanoantenna; and (d) extinction, defined as one minus the transmittance T, of an array of antennas. Light is incident at $\alpha = \theta = 0^\circ$ (red dashed curve) and $\alpha = 0^\circ, \theta = 20^\circ$ (blue solid curve).

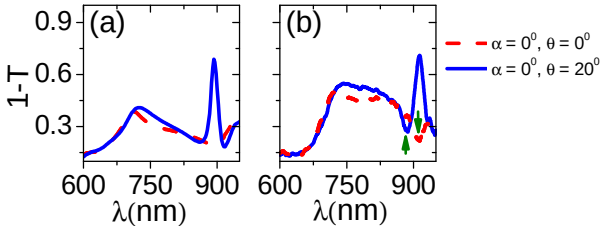

FIG. 2. (a) Calculation and (b) measurements of the optical extinction by an array of gold nanoantennas for angles of incidence $\alpha = \theta = 0^\circ$ (red dashed curve) and $\alpha = 0^\circ, \theta = 20^\circ$ (blue solid curve). The arrows in (b) indicate the Rayleigh anomalies.

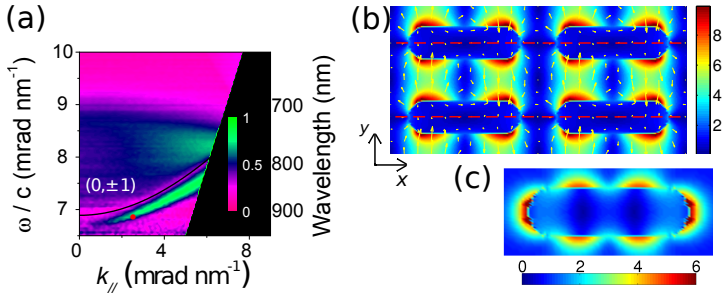

FIG. 3. (a) Extinction of an array of nanoantennas. The incident light is polarized parallel to the long axis of the antennas. The solid black curve represents the (0,±1) Rayleigh anomaly. (b) Modulus of the electric field and electric field vectors (arrows) in the (x-y) plane of the array, both calculated on the plane intersecting the nanoantennas at their middle height, $\lambda = 895$ nm and $\theta = 20°$. These wavelength and angle are indicated by the red point in (a). (c) Modulus of the electric field in a single gold nanoantenna at the frequency of the $3\lambda/2$ resonance.

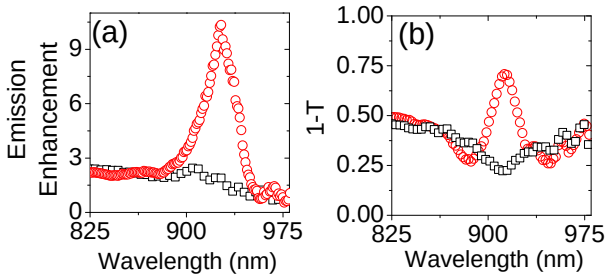

FIG. 4. (a) Fluorescence normalized by the emission in an unpatterned substrate. Black squares are measurements of the fluorescence emitted at $\alpha = \theta = 0°$, while the red circles are measurements at $\alpha = 0°, \theta = 20°$. (b) Extinction through the same array than in (a) measured at the angle of incidence $\alpha = \theta = 0°$ (black squares) and $\alpha = 0°, \theta = 20°$ (red circles).